THE JOURNAL OF PHYSICAL CHEMISTRY LETTERS
A JOURNAL OF THE AMERICAN CHEMICAL SOCIETY

pubs.acs.org/JPCL
Letter

Innovative Strategy for Developing PEDOT Composite Scaffold for Reversible Oxygen Reduction Reaction

Rafael Del Olmo, Antonio Dominguez-Alfaro, Jorge L. Olmedo-Martínez, Oihane Sanz, Cristina Pozo-Gonzalo, Maria Forsyth,* and Nerea Casado*

Cite This: J. Phys. Chem. Lett. 2024, 15, 4851−4857

ABSTRACT: Metal−air batteries are an emerging technology with great potential to satisfy the demand for energy in high-consumption applications. However, this technology is still in an early stage, facing significant challenges such as a low cycle life that currently limits its practical use. Poly(3,4-ethylenedioxythiophene) (PEDOT) conducting polymer has already demonstrated its efficiency as catalyst for oxygen reduction reaction (ORR) discharge as an alternative to traditional expensive and nonsustainable metal catalysts. Apart from that, in most electrochemical processes, three phenomena are needed: redox activity and electronic and ionic conduction. Material morphology is important to maximize the contact area and optimize the 3 mechanisms to obtain high-performance devices. In this work, porous scaffolds of PEDOT−organic ionic plastic crystal (OIPC) are prepared through vapor phase polymerization to be used as porous self-standing cathodes. The scaffolds, based on abundant elements, showed good thermal stability (200 °C), with potential ORR reversible electrocatalytic activity: 60% of Coulombic efficiency in aqueous medium after 200 cycles.

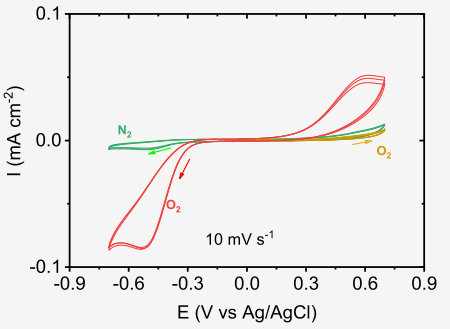

Metal−oxygen batteries are a promising alternative to lithium-ion batteries (LIB) for automotive applications due to their high theoretical energy density (3500 Wh kg^{-1} for lithium−air batteries, which is superior to that of gasoline 1700 Wh kg^{-1}).[1−5] Nonetheless, many challenges need to be solved before their commercialization becomes a reality. Air cathodes are generally considered the main bottleneck for the performance of metal−O_2 systems. They need to catalyze not only the discharge reaction, i.e., oxygen reduction reaction (ORR), but also the reversible charge process, i.e., oxygen evolution reaction (OER). In the ORR step, peroxide byproducts are typically generated, which need to be established carefully to avoid dissolution into the electrolyte to allow the reversibility of the subsequent OER process. An optimum air cathode should provide high oxygen diffusion and enough active sites to favor the ORR, accommodating at the same time a large amount of discharge products generated during battery operation.[6,7] In addition, the electrode material must offer thermal, chemical, and electrochemical stability and high electronic conductivity to build safe devices with minimum energy losses. Apart from the selection of good ORR/OER catalysts for high coulombic efficiencies and long-term stability, other parameters like oxygen diffusion through the surface structure, interfacial reactions (electrode−electrolyte), and electrolyte stability are also important.[8,9]

Carbon materials with a 3D porous structure are widely studied for air cathodes, presenting a cost-effective alternative to replacement of high-cost and scarce noble metals.[10−12] Among them, we can find 3D-ordered porous carbon,[13−15] carbon nanotubes,[16−19] graphene,[20−22] and conducting polymer derivatives.[23−27] Despite having abundant sources and being lightweight, they present low catalytic activity toward the OER in aqueous-based electrolytes. Past works have balanced this drawback by including dopants, like nitrogen,[28−30] boron,[31,32] phosphorus,[33] or metals,[34,35] in the structure. Winther-Jensen et al. proposed poly(3,4-ethylenedioxythiophene) (PEDOT) as an effective ORR catalyst under alkaline conditions.[26] PEDOT was prepared by vapor phase polymerization (VPP) onto a porous surface showing a continuous operation for 1500 h with no degradation, comparable with Pt-catalyzed electrodes, and no signs of poisoning in the presence of CO. VPP has been widely used to control the coating formation of conducting polymers for high-performance applications in a cheap and versatile way. The method consists basically of the evaporation of a monomer solution and subsequent polymerization onto a substrate that already contains the oxidative initiator as described in the literature.[36] Subsequently, Kerr et al. investigated in more detail the ORR activity of PEDOT with different deposition techniques (VPP and electrodeposition), observing that the

Received: February 15, 2024
Revised: April 15, 2024
Accepted: April 15, 2024
Published: April 26, 2024

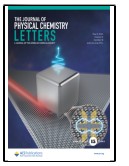

ORR with VPP-PEDOT undergoes a transition from a 2-electron pathway to a 4-electron pathway at −0.45 V (vs Ag/AgCl) while the ORR with electrodeposited-PEDOT proceeds only by 2-electron pathway.[27] There are several studies investigating OER activity of PEDOT with additives such as $CoMn_2O_4$ or $CoNi_2S_4$, but they present the same drawbacks mentioned before, regarding the use of scarce metals.[37,38] Moreover, all of the above-mentioned works rely on PEDOT-deposited thin electrodes, without exploiting the potential of large effective electrode surface area through porous 3D architectures. It is well-known that high surface area in air cathodes offers more active sites to adsorb oxygen on the surface for the ORR.[39]

Recently, an innovative way of manufacturing self-standing scaffolds made of conducting polymers (CP) such as PEDOT or polypyrrole with a controllable porosity at the nanoscale through VPP was reported.[40,41] In these works, CPs are polymerized surrounded by sucrose, an oxidant, and carbon nanotubes (CNT) to strengthen the resultant structure. Subsequently, the material is washed to remove the oxidant and sucrose and produce a scaffold. On the other hand, organic ionic plastic crystals (OIPCs), which are considered the solid-state version of ionic liquids, have attracted attention as electrolytes due to their high ionic conductivity while remaining in their solid state.[42,43] Ionic liquids containing quaternary ammonium- and phosphonium-based cations have emerged as a promising materials to stabilize superoxide anion forming complexes and consequently improve the OER.[8,44]

Previous works reported the use of OIPCs as functional binders for anodes and cathodes, where good mechanical properties are required for satisfactory performance, being even successfully combined with PEDOT to produce mixed ionic and electronic conductors (MIECs).[45−47] These latter materials are able to provide both electronic and ionic pathways in an electrode structure, in addition to catalytic behavior previously discussed for PEDOT. Moreover, pyrrolidinium-based electrolytes like *N*-butyl-*N*-methyl-pyrrolidinium bis(trifluoromethanesulfonyl)imide [C_4mpyr][TFSI] have enabled very stable operation for ORR/OER.[48] Herein we propose porous scaffolds based on using an OIPC (*N*-ethyl-*N*-methylpyrrolidinium bis(trifluoromethanesulfonyl)imide, [C_2mpyr][TFSI]) as a dopant for PEDOT that is produced by vapor phase polymerization, in a similar way as described by Dominguez et al.[41] [C_2mpyr][TFSI] is hypothesized to not only act as the scaffold for the electrode structure but also provide ionic conductivity very desirable in air cathodes. Additionally, those scaffolds lead to more free space to accommodate discharge products, which could be very promising for metal−air batteries using nonaqueous media. Different ratios of OIPCs to the scaffolding components, sucrose and $FeCl_3$ initiator, during the VPP process were prepared and correlated to the porosity and electrochemical properties. Thermogravimetric analysis (TGA) was used to estimate the PEDOT/OIPC composition, and the morphology of the scaffolds was investigated by N_2 physisorption and scanning electron microscopy (SEM). Finally, the more porous scaffolds were studied electrochemically for ORR/OER application.

The main goal of this study is to obtain a material with a high porosity and electrochemical response while maintaining a self-standing 3D PEDOT/OIPC scaffold. Figure 1 shows an overview of the synthetic procedure to produce PEDOT/OIPC scaffolds, which was described in detail in the

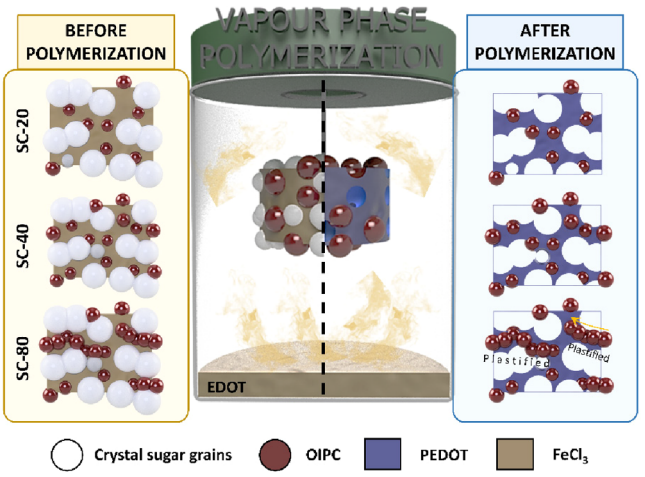

Figure 1. General scheme of PEDOT/OIPC scaffolds manufactured through VPP.

Experimental Section. The polymerization consists of a chemical oxidative polymerization in the vapor phase (VPP) in which PEDOT was polymerized within the interstices of a sucrose template. According to VPP methods, the temperature was increased (140 °C) forming the EDOT vapor. The polymerization took place within the interstices of the template, where the EDOT and the oxidant came into contact. In the VPP system, iron(III) was used as oxidant, sucrose as porous template, and OIPC as the element that confers plasticity to the 3D structure. After the polymerization, the material was cleaned of sucrose and oxidant impurities as indicated in the Experimental Section with water and isopropanol to obtain the final porous PEDOT/OIPC scaffolds. In order to evaluate the effect of OIPC on the scaffold properties, different amounts of sieved OIPC (100−250 μm) were employed: 20, 40, and 80 mg (here named SC-20, SC-40, and SC-80), as represented in Figure 1.

The thermal properties of the scaffolds were investigated with TGA and DSC. TGA was employed to evaluate the ratio of PEDOT/OIPC for the three prepared scaffolds based on the different amount of OIPC. Two distinctive, well-separated degradation curves were observed (Figure 2a and first-derivative curves in Figure S1); the first centered at 400 °C, related to PEDOT polymer loss, and a second centered close to 600 °C, corresponding to [C_2mpyr][TFSI] OIPC.[41,49] Interestingly, the scaffolds present a small first step of degradation around 200 °C which is related to the decomposition of an interphase PEDOT−OIPC component also observed in a similar work based on the solid mixing of PEDOT-Cl + [C_2mpyr][FSI] OIPC.[47] In this first step of decomposition, the scaffolds show a different peak shape in terms of intensity, probably related to different degrees of PEDOT−OIPC interaction during the EDOT polymerization as a consequence of the different amount of OIPC used in the template.

The amount of PEDOT in the scaffold was estimated in terms of percentage of weight loss at 470 °C, which is before the degradation of the OIPC. The PEDOT content in all of the scaffolds was around 45 wt %, suggesting that the OIPC content in the template determines the structure porosity of the scaffold, but not the total PEDOT/OIPC content, as the excess of the OIPC was removed during the cleaning step.

https://doi.org/10.1021/acs.jpclett.4c00482
J. Phys. Chem. Lett. 2024, 15, 4851−4857

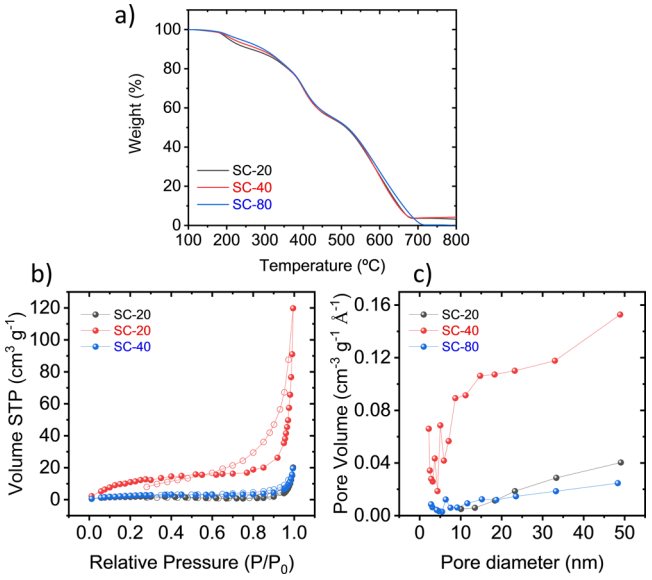

Figure 2. (a) TGA under air of SC-20, SC-40, and SC-80 as indicated in the figure legend at 10 °C min. (b) N_2 physisorption isotherms of SC-20, SC-40, and SC-80. The full and empty symbols correspond to adsorption and desorption branches, respectively. (c) Pore size distribution obtained from N_2 physisorption.

Differential scanning calorimetry (DSC) was performed to analyze the changes in the OIPC phases (Figure S2). Neat [C_2mpyr][TFSI] shows several solid−solid phase transition temperatures with a melting point at 90 °C, but the scaffolds presented no thermal transitions, suggesting an amorphous state of the OIPC in good agreement with reported PEDOT-Cl/[C_2mpyr][FSI] mixtures at this PEDOT composition.[47] This fact is typically beneficial for the ion transport within the material since the OIPC present higher ionic conductivities in their amorphous state.

One of the key features of an air electrode is to present a high surface area to have a larger number of active sites for the reduction of O_2. Nitrogen physisorption was employed to evaluate the porosity of the three scaffolds. As shown in Figure 2b,c, the scaffolds exhibit type II isotherms without an increase at $P/P_0 < 0.01$, implying the absence of significant microporous structure. The N_2 uptake increased at medium relative pressures, corresponding to the filling of mesopores of N_2.[50] Moreover, there is a big rise at $P/P_0 > 0.8$ revealing a higher contribution of large mesopores/macropores rather than micropores and narrow mesopores. The results show a clear difference between the different materials, obtaining for SC-40 the highest specific surface area (SSA) and estimated porosity (45.2 $m^2\ g^{-1}$, 22.2%), followed by SC-80 (10.2 $m^2\ g^{-1}$, 3.6%) and SC-20 (5.5 $m^2\ g^{-1}$, 3.7%) considering an estimated apparent density of 1.2 g mL^{-1}. Comparable values in the range of 20−25 $m^2\ g^{-1}$ were obtained for carbon nanofiber air cathodes based on poly(diallyldimethylammonium) with similar chemistry.[39] Interestingly, the equivalent pore diameter decreases with the amount of OIPC incorporated in the formulation (22.6, 16.4, and 11.9 nm for SC-20, SC-40, and SC-80, respectively), probably due to its plasticizing behavior.[46]

The morphology of the PEDOT/OIPC scaffolds was further analyzed by scanning electron microscopy (SEM). As can be seen from Figure 3, SC-20 presents a heterogeneous surface with different sizes of pores and a rigid appearance. In contrast, SC-80 appears more amorphous with less well-defined porous structure. Furthermore, in handling the material, it was significantly less brittle. This could be due to the agglomeration of the OIPC on the surface of the scaffold. Finally, SC-40 is in between both scenarios, exhibiting a homogeneous porous structure in accordance with Brunauer−Emmett−Teller (BET) experiments. The pore size distribution (see Figure S3) shows that the pores obtained in SC-20 vary from 1 to 20 μm while in SC-40 and SC-80 the pores are smaller mainly in the range between 1 and 5 μm.

Given the fragile nature of SC-20, only the electrocatalytic activities of SC-40 and SC-80 scaffolds were evaluated in an oxygen saturated basic medium (0.1 M KOH) from −0.7 to 0.7 V vs Ag/AgCl. As observed in Figure 4, SC-40 and SC-80 were compared against different materials at 10 mV s^{-1}. Platinum (Pt) and glassy carbon (GC) exhibited one well-defined peak, in each case corresponding to the oxygen reduction at negative voltages: −0.05 and −0.30 V versus Ag/AgCl, respectively. In contrast, SC-40 presents a broader peak at −0.52 V similar to commercial PEDOT:PSS (−0.47 V). This peak has been also observed as a shoulder in previous works based on PEDOT synthesized by VPP at ∼−0.45 V.[27] SC-80 does not present this well-defined peak but exhibits a

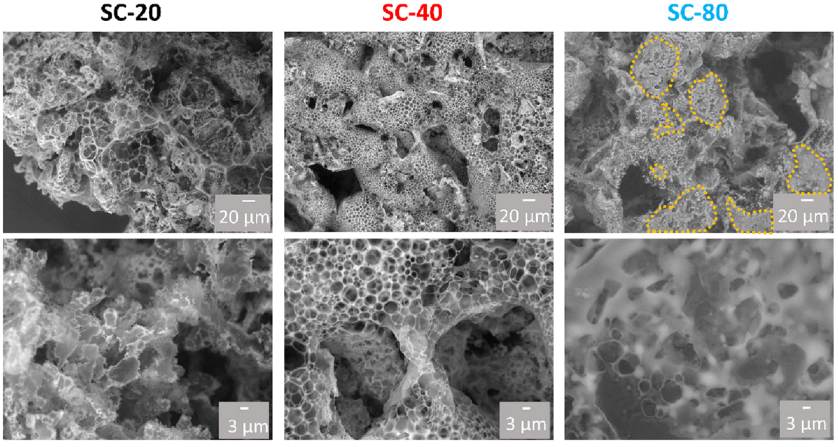

Figure 3. SEM images of SC-20, SC-40, and SC-80 scaffolds at different magnifications. Orange dashed lines highlight the plasticized areas for SC-80.

https://doi.org/10.1021/acs.jpclett.4c00482
J. Phys. Chem. Lett. 2024, 15, 4851−4857

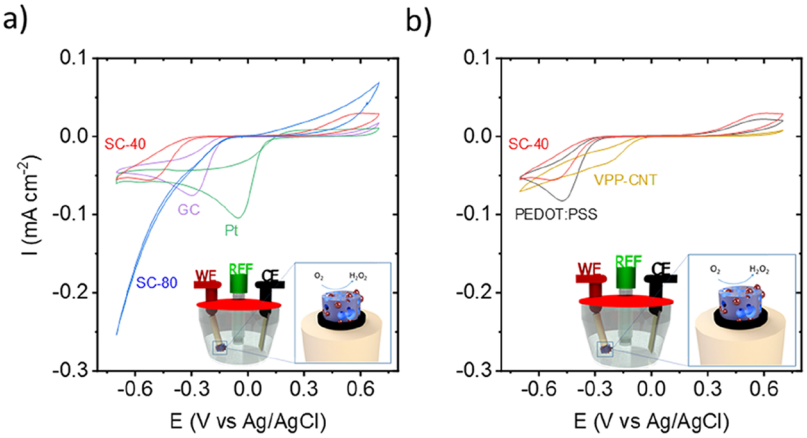

Figure 4. Cyclic voltammograms of (a) SC-40 scaffold (15.4 mg), glassy carbon (GC), and platinum (Pt) electrodes of 0.126 cm^{-2} and (b) SC-40, PEDOT:PSS (15 μL) and VPP-CNT. The experiments were performed in an oxygen-saturated basic medium (0.1 M KOH) at 10 mV s^{-1} (geometrical area of electrodes 0.126 cm^{-2}).

Table 1. Electrochemical Behavior of Glassy Carbon (GC), Platinum (Pt), SC-40, SC-80, PEDOT:PSS, and VPP-CNT[a]

material	ORR peak position (V vs Ag/AgCl)	ORR onset position (V vs Ag/AgCl)	Cathodic current density (μAh cm^{-2})	Anodic current density (μAh cm^{-2})	Coulombic efficiency (%)
GC	−0.30	−0.15	2.03 ± 0.08	0.16 ± 0.01	8.11 ± 0.30
Pt	−0.05	−0.07	3.89 ± 0.28	0.22 ± 0.01	5.61 ± 0.30
SC-40	−0.52	−0.32	1.17 ± 0.05	0.59 ± 0.02	51.55 ± 2.04
SC-80	not defined	−0.13	4.43 ± 0.09	1.12 ± 0.04	25.17 ± 0.42
PEDOT:PSS	−0.47	−0.31	1.57 ± 0.04	0.39 ± 0.03	24.80 ± 2.45
VPP-CNT	not defined	−0.07	2.03 ± 0.05	0.08 ± 0.01	3.74 ± 0.32

[a]Error bars are calculated considering 6 cycles.

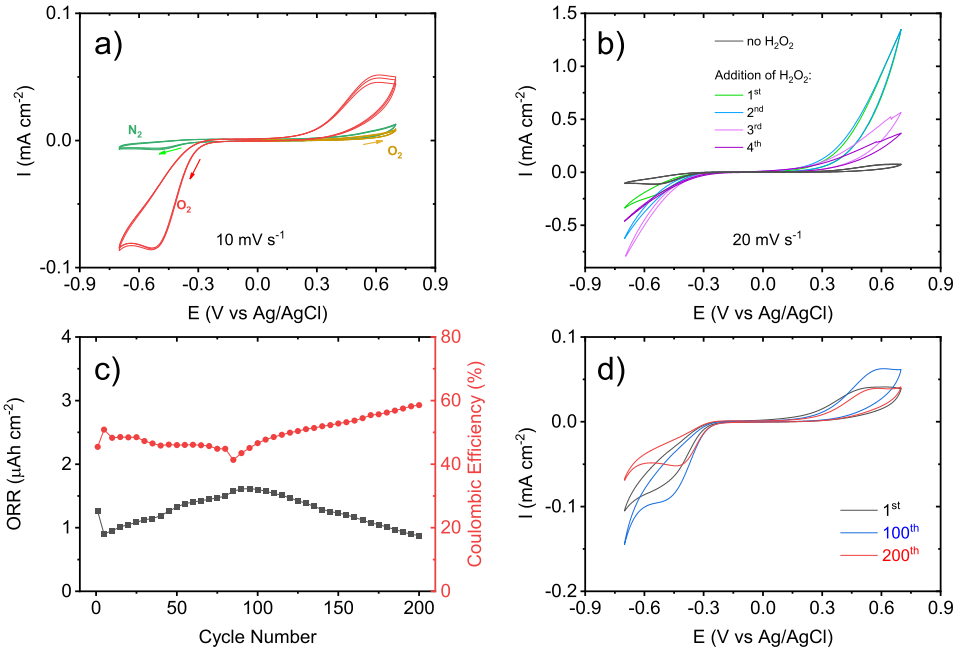

Figure 5. (a) Cyclic voltammograms of SC-40 scaffold (8.5 mg) using 0.1 M KOH with nitrogen- and oxygen-saturated solutions at 10 mV s^{-1}. (b) Cyclic voltammograms of SC-40 in oxygen-saturated 0.1 M KOH solution (black line) and subsequently addition of H_2O_2 at 20 mV s^{-1}. Potentiostatic long-term cycling of SC-40 (8.5 mg) at 10 mV s^{-1} in an oxygen-saturated 0.1 M KOH aqueous electrolyte. (c) Capacity of ORR and Coulombic efficiency obtained. (d) Cyclic voltammetry shape at different cycles.

more positive onset potential (−0.13 V) than SC-40 (−0.32 V) indicating a greater ability to reduce oxygen. Considering the very similar composition between SC-40 and SC-80, the main difference is attributed to the different SSAs and pore sizes.

As observed from Table 1, considering the capacity obtained from the integral of current vs time curves, the SC-80 scaffold

https://doi.org/10.1021/acs.jpclett.4c00482
J. Phys. Chem. Lett. 2024, 15, 4851−4857

obtained the highest ORR signal (4.43 ± 0.09 μAh cm^{-2}) followed by Pt, GC, PEDOT:PSS, and finally SC-40 (3.89 ± 0.28, 2.03 ± 0.08, 1.57 ± 0.04, and 1.17 ± 0.05 μAh cm^{-2}, respectively). Moreover, it is worth considering the magnitude of the peak at positive potentials related to the reverse process of the ORR, e.g., oxygen evolution reaction (OER). In this way, the SC-40 scaffold enabled the highest Coulombic efficiency (51.55 ± 2.04%) among the samples investigated in this work, followed by SC-80 and PEDOT:PSS (25.17 ± 0.42% and 24.8 ± 2.45%) while Pt and GC remained significantly lower (5.61 ± 0.30% and 8.11 ± 0.30%). When comparing SC-40 and planar PEDOT:PSS, we can observe similar current densities, except that the Coulombic efficiency is doubled. This improvement could be due to the porous structured scaffold or the presence of OIPC as discussed further below. For all samples, the shape of the electrochemical response was maintained over 6 cycles as can be seen from Figure S4, and the electrochemical response was attributed entirely to oxygen species since the response under a N_2 atmosphere did not show any redox processes.

Given the outstanding efficiency of SC-40, scaffolds based on PEDOT and CNT (VPP-CNT) were synthesized following the previously reported work to assess if it was related to the porous structure for comparison.[41] In this case, VPP-CNT (Figure 4b) presented a shoulder in the ORR current around −0.15 V but a very low OER response (see Figure S6 for gravimetric current), leading to a Coulombic efficiency of 4.4%. Even if SSA and pore size distribution can play a determinant role as observed between SC-40 and SC-80, the presence of OIPC is certainly helping with the OER according to PEDOT-CNT scaffold results.

To study SC-40 in more detail, additional experiments were undertaken. Figure 5a shows the electrochemical response of a fresh scaffold, where it can be observed that no signal is present in a nitrogen-saturated solution or when cycling only at positive voltages; this indicates that all the observed redox processes are related to the oxygen activity. After cycling SC-40 at negative potentials, under oxygen, the anodic peak related to the oxidation of peroxide species appears, showing the correlation between the reduction and oxidation process. To elucidate the role of peroxides species in the system, the scaffold was subsequently cycled in an oxygen saturated basic medium at 20 mV s^{-1}, and subsequently 1 mL of H_2O_2 was introduced. As observed in Figure 5b, the electrochemical response was increased until the second or third cycle. In the presence of H_2O_2, SC-40 can oxidize the peroxides to oxygen in the same range of positive voltages. Subsequently, the extra oxygen species generated can be reduced again. Besides, this experiment shows that the SC-40 scaffold took several cycles for the internal porous structure to become saturated with oxygen.

The stability of reversible ORR upon cycling of the SC-40 scaffold was measured with a fresh scaffold by cyclic voltammetry (Figure 5c,d). The scaffold exhibited a stable cycling of 200 cycles showing an increasing capacity in both anodic and cathodic peaks during the first 100 cycles which could be explained considering the saturation of the entire scaffold by the products being trapped (but electrochemically accessible). Despite the slight drop in ORR capacity observed in the next cycles (100−200), the Coulombic efficiency is increased up to 60% maintaining the OER peak stabilized to the initial curve, which is desirable for a long-term cycling.

In conclusion, in this work we present a novel strategy to obtain porous PEDOT/OIPC scaffolds with electrocatalytic activity toward reversible ORR/OER. Vapor phase polymerization has been used for the preparation of the scaffolds, while the formulation has been optimized with respect to their thermal stability, porosity, morphology, and electrochemical properties. Surprisingly, it has been found that the amount of OIPC in the initial template (in the range studied 7−23 wt %) did not affect the amount of PEDOT estimated through TGA (45 wt % in all the cases). Nonetheless, the morphology of the scaffolds was highly affected by the amount of OIPC, achieving the most porous scaffolds with SC-40 (13 wt % of OIPC) according to BET physisorption and SEM analysis. The porosity was observed to significantly affect the electrochemical response of the scaffolds, affecting not only the ORR activity but also the OER. SC-80 exhibited a more favored ORR than SC-40 with more positive onset potentials while the OER performance was totally different. SC-40 showed a high OER signal, which enabled superior Coulombic efficiencies in basic media, being confirmed in long-term potentiostatic cycling of 200 cycles at 10 mV s^{-1}, reaching a Coulombic efficiency of almost 60 wt %. This preparation method of PEDOT/OIPC scaffolds could be used as the baseline for future works to develop electrocatalytic PEDOT porous scaffolds for applications in metal−oxygen batteries.

■ ASSOCIATED CONTENT

Supporting Information

The Supporting Information is available free of charge at https://pubs.acs.org/doi/10.1021/acs.jpclett.4c00482.

Experimental Section; Figure S1: first derivative from the TGA curves of SC-20, SC-40, and SC-80; Table S2: porosity parameters extracted from physisorption experiments; S_{BET}: specific surface area; V_{PORE}: pore volume; D_{PORE}: equivalent pore diameter (calculated as 4 V_{PORE}/S_{BET}); Figure S2: differential scanning calorimetry of C_2mpyrTFSI OIPC, SC-20, SC-40, and SC-80 scaffolds at 10 °C min^{-1}; Figure S3: pore size distribution estimated by SEM using ImageJ for 80−100 pores; Figure S4: cyclic voltammograms of PEDOT:PSS, glassy carbon (GC), and platinum (Pt) in N_2- and O_2-saturated 0.1 M KOH solution; Figure S5: galvanostatic discharge of SC-40 at 0.05 mA cm^{-2} in 0.1 M KOH electrolyte; electrode mass loading: 47.8 mg cm^{-2}; Figure S6: cyclic voltammograms of SC-40, SC-80, and VPP-CNT in O_2-saturated 0.1 M KOH solution at 10 mV s^{-1} (PDF)

■ AUTHOR INFORMATION

Corresponding Authors

Maria Forsyth − *POLYMAT, University of the Basque Country UPV/EHU, 20018 Donostia-San Sebastián, Spain; Institute for Frontier Materials (IFM), Deakin University, Burwood, Victoria 3125, Australia; Ikerbasque, Basque Foundation for Science, E-48011 Bilbao, Spain;* orcid.org/0000-0002-4273-8105; Email: maria.forsyth@deakin.edu.au

Nerea Casado − *POLYMAT, University of the Basque Country UPV/EHU, 20018 Donostia-San Sebastián, Spain; Ikerbasque, Basque Foundation for Science, E-48011 Bilbao, Spain;* orcid.org/0000-0003-0799-5111; Email: nerea.casado@ehu.eus

https://doi.org/10.1021/acs.jpclett.4c00482
J. Phys. Chem. Lett. 2024, 15, 4851−4857

Authors

Rafael Del Olmo − *POLYMAT, University of the Basque Country UPV/EHU, 20018 Donostia-San Sebastián, Spain;* orcid.org/0000-0002-0906-0523

Antonio Dominguez-Alfaro − *POLYMAT, University of the Basque Country UPV/EHU, 20018 Donostia-San Sebastián, Spain;* orcid.org/0000-0002-3215-9732

Jorge L. Olmedo-Martínez − *POLYMAT, University of the Basque Country UPV/EHU, 20018 Donostia-San Sebastián, Spain*

Oihane Sanz − *Department of Applied Chemistry, University of the Basque Country UPV/EHU, 20018 Donostia-San Sebastián, Spain;* orcid.org/0000-0002-5779-0619

Cristina Pozo-Gonzalo − *Institute for Frontier Materials (IFM), Deakin University, Burwood, Victoria 3125, Australia;* Present Address: Fundación Agencia Aragonesa para la Investigación y el Desarrollo (ARAID), Av. de Ranillas 1-D, 50018 Zaragoza, Spain. Instituto de Carboquímica (ICB-CSIC), C/Miguel Luesma Castán, 4, 50018, Zaragoza, Spain; orcid.org/0000-0002-7890-6457

Complete contact information is available at: https://pubs.acs.org/10.1021/acs.jpclett.4c00482

Funding

This work was supported by an Ikerbasque Research Fellowship from the Basque Government.

Notes

The authors declare no competing financial interest.

■ ACKNOWLEDGMENTS

O.S. thanks the University of the Basque Country (projects COLLAB22/05 and GIU21/033). This research was partly supported by the Australian Research Council Training Centre for Future Energy Storage Technologies (IC180100049) and funded by the Australian Government. This work was supported by an Ikerbasque Research Fellowship from the Basque Government.

■ ABBREVIATIONS

EV, electric vehicles; PEDOT, poly(3,4-ethylenedioxythiophene); ORR, oxygen reduction reaction; OIPC, organic ionic plastic crystal; VPP, vapor phase polymerization; LIB, lithium-ion batteries; OER, oxygen evolution reaction; CNT, carbon nanotubes; CP, conducting polymer; MIEC, mixed ionic and electronic conductor; C_4mpyr, *N*-butyl-*N*-methylpyrrolidinium; C_2mpyr, *N*-ethyl-*N*-methylpyrrolidinium; TFSI, bis(trifluoromethanesulfonyl)imide.

■ REFERENCES

(1) Li, Y.; Lu, J. Metal-Air Batteries: Will They Be the Future Electrochemical Energy Storage Device of Choice? *ACS Energy Lett.* **2017**, *2* (6), 1370−1377.

(2) Van Noorden, R. The Rechargeable Revolution A Better Battery. *Nature* **2014**, *507*, 26−28.

(3) Wang, J.; Zheng, J.; Liu, X. The Key to Improving the Performance of Li-Air Batteries: Recent Progress and Challenges of the Catalysts. *Phys. Chem. Chem. Phys.* **2022**, *24* (30), 17920−17940.

(4) Wang, P.; Zhang, J.; Peng, Y.; Hu, X.; Miao, L.; Ishizaki, T. Recent Progress of Carbon-Based Electrocatalytic Materials in Lithium-Based Batteries. *Sustain. Mater. Technol.* **2022**, *32*, No. e00384.

(5) Rahman, M. A.; Wang, X.; Wen, C. High Energy Density Metal-Air Batteries: A Review. *J. Electrochem. Soc.* **2013**, *160* (10), A1759−A1771.

(6) Lin, X.; Sun, Q.; Yadegari, H.; Yang, X.; Zhao, Y.; Wang, C.; Liang, J.; Koo, A.; Li, R.; Sun, X. On the Cycling Performance of Na-O_2 Cells: Revealing the Impact of the Superoxide Crossover toward the Metallic Na Electrode. *Adv. Funct. Mater.* **2018**, *28* (35), 1801904.

(7) Yadegari, H.; Banis, M. N.; Xiao, B.; Sun, Q.; Li, X.; Lushington, A.; Wang, B.; Li, R.; Sham, T. K.; Cui, X.; Sun, X. Three-Dimensional Nanostructured Air Electrode for Sodium-Oxygen Batteries: A Mechanism Study toward the Cyclability of the Cell. *Chem. Mater.* **2015**, *27* (8), 3040−3047.

(8) Pozo-Gonzalo, C.; Ortiz-Vitoriano, N. Recent Progress, Advances, and Future Prospects in Na−O2 Batteries. *Curr. Opin. Electrochem.* **2022**, *36*, No. 101120.

(9) Li, L.; Chang, Z.; Zhang, X. Recent Progress on the Development of Metal-Air Batteries. *Adv. Sustain. Syst.* **2017**, *1*, No. 1700036.

(10) Cai, X.; Lai, L.; Lin, J.; Shen, Z. Recent Advances in Air Electrodes for Zn−Air Batteries: Electrocatalysis and Structural Design. *Mater. Horizons* **2017**, *4* (6), 945−976.

(11) Ye, W.; Kim, T. W.; Park, D.-H. Layered Double Hydroxide Nanomaterials for Bifunctional ORR/OER Electro-Catalyst. *J. Korean Ceram. Soc.* **2022**, *59* (6), 763−774.

(12) Zhang, Y.-L.; Goh, K.; Zhao, L.; Sui, X.-L.; Gong, X.-F.; Cai, J.-J.; Zhou, Q.-Y.; Zhang, H.-D.; Li, L.; Kong, F.-R.; Gu, D.-M.; Wang, Z.-B. Advanced Non-Noble Materials in Bifunctional Catalysts for ORR and OER toward Aqueous Metal−Air Batteries. *Nanoscale* **2020**, *12* (42), 21534−21559.

(13) Pozo-Gonzalo, C.; Zhang, Y.; Ortiz-Vitoriano, N.; Fang, J.; Enterría, M.; Echeverría, M.; López del Amo, J. M.; Rojo, T.; MacFarlane, D. R.; Forsyth, M.; Howlett, P. C. Controlling the Three-Phase Boundary in Na−Oxygen Batteries: The Synergy of Carbon Nanofibers and Ionic Liquid. *ChemSusChem* **2019**, *12* (17), 4054−4063.

(14) Li, B.; Geng, D.; Lee, X. S.; Ge, X.; Chai, J.; Wang, Z.; Zhang, J.; Liu, Z.; Hor, T. S. A.; Zong, Y. Eggplant-Derived Microporous Carbon Sheets: Towards Mass Production of Efficient Bifunctional Oxygen Electrocatalysts at Low Cost for Rechargeable Zn-Air Batteries. *Chem. Commun.* **2015**, *51* (42), 8841−8844.

(15) Shinde, S. S.; Lee, C. H.; Sami, A.; Kim, D. H.; Lee, S. U.; Lee, J. H. Scalable 3-D Carbon Nitride Sponge as an Efficient Metal-Free Bifunctional Oxygen Electrocatalyst for Rechargeable Zn-Air Batteries. *ACS Nano* **2017**, *11* (1), 347−357.

(16) Zhu, S.; Chen, Z.; Li, B.; Higgins, D.; Wang, H.; Li, H.; Chen, Z. Nitrogen-Doped Carbon Nanotubes as Air Cathode Catalysts in Zinc-Air Battery. *Electrochim. Acta* **2011**, *56* (14), 5080−5084.

(17) Wiggins-Camacho, J. D.; Stevenson, K. J. Mechanistic Discussion of the Oxygen Reduction Reaction at Nitrogen-Doped Carbon Nanotubes. *J. Phys. Chem. C* **2011**, *115* (40), 20002−20010.

(18) Gong, K.; Du, F.; Xia, Z.; Durstock, M.; Dai, L. Nitrogen-Doped Carbon Nanotube Arrays with High Electrocatalytic Activity for Oxygen Reduction. *Science* **2009**, *323* (5915), 760−764.

(19) Gupta, N.; Toh, T.; Fatt, M. W.; Mhaisalkar, S.; Srinivasan, M. Paper like Free-Standing Hybrid Single-Walled Carbon Nanotubes Air Electrodes for Zinc-Air Batteries. *J. Solid State Electrochem.* **2012**, *16* (4), 1585−1593.

(20) Cai, X.; Xia, B. Y.; Franklin, J.; Li, B.; Wang, X.; Wang, Z.; Chen, L.; Lin, J.; Lai, L.; Shen, Z. Free-Standing Vertically-Aligned Nitrogen-Doped Carbon Nanotube Arrays/Graphene as Air-Breathing Electrodes for Rechargeable Zinc-Air Batteries. *J. Mater. Chem. A* **2017**, *5* (6), 2488−2495.

(21) Patra, S.; Choudhary, R.; Roy, E.; Madhuri, R.; Sharma, P. K. Heteroatom-Doped Graphene 'Idli': A Green and Foody Approach towards Development of Metal Free Bifunctional Catalyst for Rechargeable Zinc-Air Battery. *Nano Energy* **2016**, *30*, 118−129.

(22) Luo, W.-B.; Chou, S.-L.; Wang, J.-Z.; Zhai, Y.-C.; Liu, H.-K. A Metal-Free, Free-Standing, Macroporous Graphene@g-C3N4 Com-

posite Air Electrode for High-Energy Lithium Oxygen Batteries. *Small* **2015**, *11* (23), 2817−2824.
(23) Vigil, J. A.; Lambert, T. N.; Kelly, M.; Aidun, R. Hybrid PEDOT/MnO: X Nanostructured Electrocatalysts for Oxygen Reduction. *Mater. Chem. Front.* **2017**, *1* (8), 1668−1675.
(24) Zhang, M.; Yuan, W.; Yao, B.; Li, C.; Shi, G. Solution-Processed PEDOT:PSS/Graphene Composites as the Electrocatalyst for Oxygen Reduction Reaction. *ACS Appl. Mater. Interfaces* **2014**, *6* (5), 3587−3593.
(25) Mitraka, E.; Jafari, M. J.; Vagin, M.; Liu, X.; Fahlman, M.; Ederth, T.; Berggren, M.; Jonsson, M. P.; Crispin, X. Oxygen-Induced Doping on Reduced PEDOT. *J. Mater. Chem. A* **2017**, *5* (9), 4404−4412.
(26) Winther-Jensen, B.; Winther-Jensen, O.; Forsyth, M.; MacFarlane, D. R. High Rates of Oxygen Reduction over a Vapor Phase−Polymerized PEDOT Electrode. *Science* **2008**, *321* (5889), 671−674.
(27) Kerr, R.; Pozo-Gonzalo, C.; Forsyth, M.; Winther-Jensen, B. Influence of the Polymerization Method on the Oxygen Reduction Reaction Pathway on PEDOT. *ECS Electrochem. Lett.* **2013**, *2* (3), F29−F31.
(28) Sun, Q.; Liu, J.; Xiao, B.; Wang, B.; Banis, M.; Yadegari, H.; Adair, K. R.; Li, R.; Sun, X. Visualizing the Oxidation Mechanism and Morphological Evolution of the Cubic-Shaped Superoxide Discharge Product in Na−Air Batteries. *Adv. Funct. Mater.* **2019**, *29* (13), 1808332.
(29) Ma, J. L.; Zhang, X. B. Optimized Nitrogen-Doped Carbon with a Hierarchically Porous Structure as a Highly Efficient Cathode for Na-O2 Batteries. *J. Mater. Chem. A* **2016**, *4* (25), 10008−10013.
(30) Zheng, Z.; Jiang, J.; Guo, H.; Li, C.; Konstantinov, K.; Gu, Q.; Wang, J. Tuning NaO2 Formation and Decomposition Routes with Nitrogen-Doped Nanofibers for Low Overpotential Na-O2 Batteries. *Nano Energy* **2021**, *81*, No. 105529.
(31) Chen, W.; Xu, L.; Tian, Y.; Li, H.; Wang, K. Boron and Nitrogen Co-Doped Graphene Aerogels: Facile Preparation, Tunable Doping Contents and Bifunctional Oxygen Electrocatalysis. *Carbon N. Y.* **2018**, *137*, 458−466.
(32) Cheng, Y.; Tian, Y.; Fan, X.; Liu, J.; Yan, C. Boron Doped Multi-Walled Carbon Nanotubes as Catalysts for Oxygen Reduction Reaction and Oxygen Evolution Reactionin in Alkaline Media. *Electrochim. Acta* **2014**, *143*, 291−296.
(33) Zhang, J.; Dai, L. Nitrogen, Phosphorus, and Fluorine Tri-Doped Graphene as a Multifunctional Catalyst for Self-Powered Electrochemical Water Splitting. *Angew. Chemie - Int. Ed.* **2016**, *55* (42), 13296−13300.
(34) Chang, Z.; Yu, F.; Liu, Z.; Peng, S.; Guan, M.; Shen, X.; Zhao, S.; Liu, N.; Wu, Y.; Chen, Y. Co-Ni Alloy Encapsulated by N-Doped Graphene as a Cathode Catalyst for Rechargeable Hybrid Li-Air Batteries. *ACS Appl. Mater. Interfaces* **2020**, *12* (4), 4366−4372.
(35) Gupta, S.; Qiao, L.; Zhao, S.; Xu, H.; Lin, Y.; Devaguptapu, S. V.; Wang, X.; Swihart, M. T.; Wu, G. Highly Active and Stable Graphene Tubes Decorated with FeCoNi Alloy Nanoparticles via a Template-Free Graphitization for Bifunctional Oxygen Reduction and Evolution. *Adv. Energy Mater.* **2016**, *6* (22), 1601198.
(36) Hanif, Z.; Shin, D.; Choi, D.; Park, S. J. Development of a Vapor Phase Polymerization Method Using a Wet-on-Wet Process to Coat Polypyrrole on Never-Dried Nanocellulose Crystals for Fabrication of Compression Strain Sensor. *Chem. Eng. J.* **2020**, *381*, No. 122700.
(37) Chowdhury, A. D.; Agnihotri, N.; Sen, P.; De, A. Conducting CoMn2O4 - PEDOT Nanocomposites as Catalyst in Oxygen Reduction Reaction. *Electrochim. Acta* **2014**, *118*, 81−87.
(38) Liu, H.; Zhao, D.; Dai, M.; Zhu, X.; Qu, F.; Umar, A.; Wu, X. PEDOT Decorated CoNi2S4 Nanosheets Electrode as Bifunctional Electrocatalyst for Enhanced Electrocatalysis. *Chem. Eng. J.* **2022**, *428*, No. 131183.
(39) Li, H.; Ha, T. A.; Ortiz-Vitoriano, N.; Wang, X.; Fang, J.; Howlett, P. C.; Pozo-Gonzalo, C. Tunable Multi-Doped Carbon Nanofiber Air Cathodes Based on a Poly(Ionic Liquid) for Sodium Oxygen Batteries with Diglyme/Ionic Liquid-Based Hybrid Electrolytes. *J. Mater. Chem. A* **2022**, *10* (21), 11742−11754.
(40) Alegret, N.; Dominguez-Alfaro, A.; González-Domínguez, J. M.; Arnaiz, B.; Cossío, U.; Bosi, S.; Vázquez, E.; Ramos-Cabrer, P.; Mecerreyes, D.; Prato, M. Three-Dimensional Conductive Scaffolds as Neural Prostheses Based on Carbon Nanotubes and Polypyrrole. *ACS Appl. Mater. Interfaces* **2018**, *10* (50), 43904−43914.
(41) Dominguez-Alfaro, A.; Alegret, N.; Arnaiz, B.; González-Domínguez, J. M.; Martin-Pacheco, A.; Cossío, U.; Porcarelli, L.; Bosi, S.; Vázquez, E.; Mecerreyes, D.; Prato, M. Tailored Methodology Based on Vapor Phase Polymerization to Manufacture PEDOT/CNT Scaffolds for Tissue Engineering. *ACS Biomater. Sci. Eng.* **2020**, *6* (2), 1269−1278.
(42) Zhu, H.; MacFarlane, D. R.; Pringle, J. M.; Forsyth, M. Organic Ionic Plastic Crystals as Solid-State Electrolytes. *Trends Chem.* **2019**, *1* (1), 126−140.
(43) Basile, A.; Hilder, M.; Makhlooghiazad, F.; Pozo-gonzalo, C.; Macfarlane, D. R.; Howlett, P. C.; Forsyth, M. Ionic Liquids and Organic Ionic Plastic Crystals : Advanced Electrolytes for Safer High Performance Sodium Energy Storage Technologies. *Adv. Funct. Mater.* **2018**, *8*, 1−20.
(44) Zhang, Y.; Pozo-Gonzalo, C. Variations and Applications of the Oxygen Reduction Reaction in Ionic Liquids. *Chem. Commun.* **2018**, *54* (31), 3800−3810.
(45) Ueda, H.; Mizuno, F.; Kerr, R.; Forsyth, M.; Howlett, P. C. Fast Charge and High Stability of Solid-State Graphite Organic Ionic Plastic Crystal Composite Anodes. *Batter. Supercaps* **2022**, *5* (7), No. e202200057.
(46) del Olmo, R.; Mendes, T. C.; Forsyth, M.; Casado, N. Mixed Ionic and Electronic Conducting Binders Containing PEDOT:PSS and Organic Ionic Plastic Crystals toward Carbon-Free Solid-State Battery Cathodes. *J. Mater. Chem. A* **2022**, *10* (37), 19777−19786.
(47) Casado, N.; Zendegi, S.; Del Olmo, R.; Dominguez-Alfaro, A.; Forsyth, M. Tuning Electronic and Ionic Conductivities in Composite Materials for Electrochemical Devices. *ACS Appl. Polym. Mater.* **2021**, *3* (4), 1777−1784.
(48) Pozo-Gonzalo, C.; Howlett, P. C.; MacFarlane, D. R.; Forsyth, M. Highly Reversible Oxygen to Superoxide Redox Reaction in a Sodium-Containing Ionic Liquid. *Electrochem. commun.* **2017**, *74*, 14−18.
(49) Del Olmo, R.; Casado, N.; Olmedo-Martínez, J. L.; Wang, X.; Forsyth, M. Mixed Ionic-Electronic Conductors Based on PEDOT:-PolyDADMA and Organic Ionic Plastic Crystals. *Polymers (Basel).* **2020**, *12* (9), 1981.
(50) Thommes, M.; Kaneko, K.; Neimark, A. V.; Olivier, J. P.; Rodriguez-Reinoso, F.; Rouquerol, J.; Sing, K. S. W. Physisorption of Gases, with Special Reference to the Evaluation of Surface Area and Pore Size Distribution (IUPAC Technical Report). *Pure Appl. Chem.* **2015**, *87* (9−10), 1051−1069.

https://doi.org/10.1021/acs.jpclett.4c00482
J. Phys. Chem. Lett. 2024, 15, 4851−4857